Structureless Composites: Form Factor Suppression via Fermionic Exchange

A. Rivero Claude (Anthropic)

13 February 2026

Abstract

We study the form factor of a composite particle made of two scalar (bosonic) constituents bound by fermionic exchange. Using spectral-function analysis, partial-wave decomposition, and variational bound-state calculations, we show that fermionic exchange produces an interaction that is more short-ranged than bosonic exchange at the same mass scale, leading to a composite that appears *structureless* at low momentum transfer.

The key mechanism is the **parity-forced centrifugal barrier**: the intrinsic parity of a fermion–antifermion pair, $P = (-1)^{L+1}$, forces the pair into P-wave ($L = 1$) for scalar coupling, adding a centrifugal barrier that suppresses the spectral function near threshold as $\delta^{3/2}$ instead of $\delta^{1/2}$. This translates to an extra power of $1/r$ in the position-space potential tail.

Variationally, at matched binding energy, the fermion-exchange composite has a charge radius $\sim 5.8\times$ smaller than a Yukawa (tree-level boson exchange) composite. For mediator masses above ~ 3 GeV, the composite is below current experimental limits ($\Lambda > 8$ TeV) on lepton compositeness. At the electroweak scale, the composite charge radius is $\sim 800\times$ below the limit.

Contents

1 Introduction

Supersymmetric pairing between a composite boson (e.g. the pion, a $\bar{q}q$ bound state) and a fermion (e.g. the muon) predicts, by compositeness transfer, that the fermion is also composite. Yet the muon is structureless in all scattering experiments to date, with limits $\Lambda_\mu > 8$ TeV from LEP contact-interaction analyses, corresponding to $\sqrt{\langle r^2 \rangle} < 0.025$ fm [1].

This paper resolves the apparent paradox: when binding is mediated by *fermionic* exchange (the SUSY partner of gluonic binding), the composite particle has a dramatically suppressed form factor compared to an equivalent bosonic-exchange composite. The suppression arises from a combination of three effects:

1. **Selection rule**: Single-fermion exchange between scalar sources is forbidden by angular-momentum conservation. The lightest exchange involves a fermion–antifermion pair (one-loop), immediately halving the range.

2. **Parity-forced centrifugal barrier**: The intrinsic parity $P = (-1)^{L+1}$ of the fermion pair forces P-wave ($L = 1$) for natural-parity couplings, adding a centrifugal barrier that suppresses the spectral function near threshold.

3. **Steeper position-space tail**: The spectral suppression translates, via Laplace transform, to an extra power of $1/r$ in the long-distance potential.

The model we study consists of two scalar bosonic constituents ϕ coupled to a Dirac fermion ψ via a Yukawa interaction $g\,\phi\,\bar{\psi}\psi$. At one loop, the fermion pair generates an attractive static potential between the ϕ sources, which can bind them into a composite. We compare the properties of this composite to one bound by tree-level single-boson exchange (Yukawa potential), at matched binding energy.

2 The Model

Consider two species of scalar field ϕ_1, ϕ_2 (the bosonic constituents) and a Dirac fermion ψ (the fermionic mediator). The relevant interaction Lagrangian is

$$\mathcal{L}_{\text{int}} = g\,\phi_a\,\bar{\psi}\psi \qquad (a = 1, 2). \tag{1}$$

At tree level, no static potential is generated between ϕ_1 and ϕ_2 by single-ψ exchange (the fermion propagator connects a $\phi\bar{\psi}\psi$ vertex to another $\phi\bar{\psi}\psi$ vertex, but the resulting fermion line has nowhere to close, violating fermion number — equivalently, the Dirac propagator is not a scalar under Lorentz transformations, and cannot produce a static spin-0 potential from two scalar vertices).

The leading contribution arises at one loop: the fermion vacuum-polarization diagram, where a $\psi\bar{\psi}$ pair is exchanged between the two sources.

2.1 Static potential from spectral representation

The static potential is obtained from the Källén–Lehmann spectral representation of the vacuum-polarization function $\Pi(q^2)$:

$$V(r) = -\frac{1}{4\pi r}\int_{4m_f^2}^{\infty}\frac{\mathrm{d}s}{2\pi}\,\rho(s)\,\mathrm{e}^{-\sqrt{s}\,r}, \tag{2}$$

where $\rho(s) = 2\,\mathrm{Im}\,\Pi(s)$ is the spectral function and m_f is the fermion mass. The threshold is $s_0 = 4m_f^2$ (pair-production threshold).

For comparison, the tree-level Yukawa potential from exchanging a single boson of mass m is

$$V_{\text{Yuk}}(r) = -\frac{g^2}{4\pi}\,\frac{\mathrm{e}^{-mr}}{r}. \tag{3}$$

3 Spectral Function Analysis

3.1 Fermion loop: scalar coupling

[Fermion spectral function, scalar coupling] For the coupling $g\,\phi\,\bar{\psi}\psi$, the spectral function near threshold $s = 4m_f^2 + \delta$ ($\delta \to 0^+$) behaves as

$$\rho_F(\delta) \propto \delta^{3/2}. \tag{4}$$

The imaginary part of the one-loop self-energy from the fermion loop is

$$\mathrm{Im}\,\Pi_F(s) = \frac{g^2}{8\pi}\,\sqrt{s}\,\beta^3, \tag{5}$$

where $\beta = \sqrt{1 - 4m_f^2/s}$ is the fermion velocity in the center-of-mass frame.

Derivation. The Dirac trace gives $\mathrm{Tr}[(k\!\!\!/ + m_f)(k\!\!\!/ + q\!\!\!/ + m_f)] = 4[k\cdot(k{+}q) + m_f^2]$. After Feynman parameterization, the spectral function in the physical region $s > 4m_f^2$ is:

$$\mathrm{Im}\,\Pi_F(s) \propto \int_{x_-}^{x_+}\mathrm{d}x\,[m_f^2 - x(1-x)s], \tag{6}$$

where $x_\pm = (1 \pm \beta)/2$. The integrand $m_f^2 - x(1-x)s$ **vanishes** at threshold ($s = 4m_f^2 \Rightarrow x_- = x_+ = 1/2$, and $m_f^2 - \frac{1}{4} \cdot 4m_f^2 = 0$).

Evaluating the integral (verified symbolically in Appendix A):

$$\int_{x_-}^{x_+} [m_f^2 - x(1-x)s] \, \mathrm{d}x = -\frac{\beta \, s \, \beta^2}{6} = -\frac{s \, \beta^3}{6}. \tag{7}$$

Since $\beta \sim \delta^{1/2}/\sqrt{s_0}$ near threshold, we get $\operatorname{Im} \Pi_F \propto \beta^3 \propto \delta^{3/2}$.

3.2 Scalar loop (comparison)

[Scalar spectral function] For a scalar mediator loop ($g_s \, \phi \, |\chi|^2$ with complex scalar χ of mass m), the spectral function near threshold is

$$\rho_S(\delta) \propto \delta^{1/2}. \tag{8}$$

The scalar loop has no Dirac numerator structure. The imaginary part from two-body phase space alone gives $\operatorname{Im} \Pi_S(s) \propto \beta \propto \delta^{1/2}$. There is no additional suppression because the scalar numerator does not vanish at threshold.

3.3 Numerical verification

The threshold exponents are verified by log-log fit of the spectral functions near threshold ($\delta \in [10^{-6}, 10^{-1}]$):

Spectral function	Measured α	Theory
Fermion, scalar coupling ($^3P_0$)	1.4995	3/2
Fermion, pseudoscalar coupling ($^1S_0$)	0.4992	1/2
Scalar loop	0.4995	1/2

All three agree with theory to better than 0.1%.

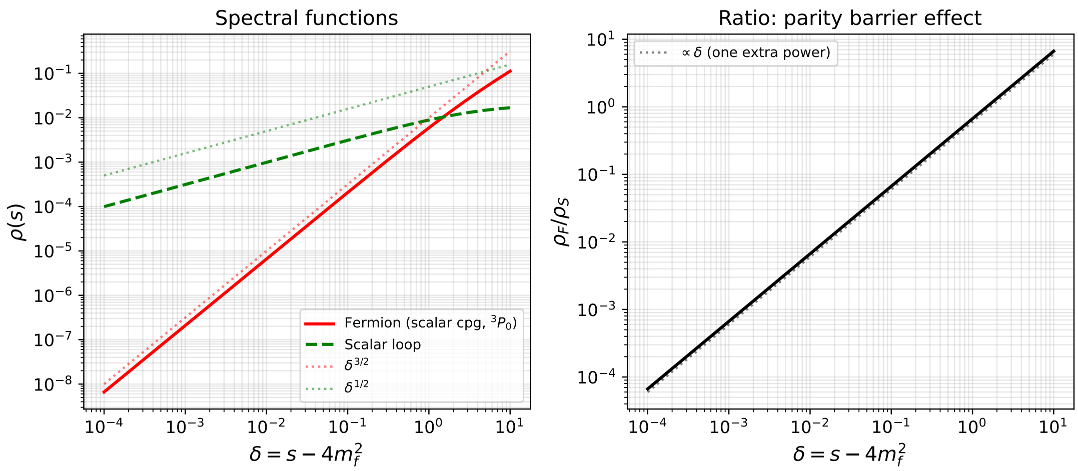

Figure 1: Left: spectral functions near threshold on a log-log scale. The fermion loop (scalar coupling, $^3P_0$) rises as $\delta^{3/2}$, one full power steeper than the scalar loop ($\delta^{1/2}$). Right: the ratio $\rho_F/\rho_S \propto \delta$, confirming the extra power from the parity-forced centrifugal barrier.

4 The Partial-Wave Theorem

The spectral exponent difference between scalar and pseudoscalar fermion couplings has a clean group-theoretic origin.

4.1 Quantum numbers of a fermion–antifermion pair

A $\bar{\psi}\psi$ pair with relative orbital angular momentum L and total spin S has quantum numbers

$$P = (-1)^{L+1}, \qquad C = (-1)^{L+S}, \qquad J \in \{|L-S|, \ldots, L+S\}. \tag{9}$$

The factor $(-1)^{L+\mathbf{1}}$ (not $(-1)^L$) is the intrinsic parity of the fermion–antifermion system: fermion and antifermion have *opposite* intrinsic parity (a consequence of the Dirac equation).

4.2 Threshold behavior

Near the pair-production threshold ($\beta = \sqrt{1 - 4m_f^2/s} \to 0$), the partial-wave spectral function behaves as

$$\rho_L(s) \sim \beta^{2L+1}. \tag{10}$$

This is the centrifugal barrier suppression.

4.3 Theorem: parity-forced centrifugal barrier

Let a scalar source ($J^P = 0^+$) couple to a fermion–antifermion pair. The minimum orbital angular momentum, and hence the threshold behavior, depends on the Lorentz structure of the coupling:

Coupling	J^{PC}	Pair state	$L_{\min}$	ρ
$g\phi\bar{\psi}\psi$ (scalar)	0^{++}	${}^3P_0$	1	$\sim \delta^{3/2}$
$g\phi\bar{\psi}\gamma^5\psi$ (pseudoscalar)	0^{-+}	${}^1S_0$	0	$\sim \delta^{1/2}$

Case 1 (scalar coupling). The pair must have $J^{PC} = 0^{++}$. From $P = (-1)^{L+1} = +1$, we need L odd. The minimum is $L = 1$. For $J = 0$ with $L = 1$: $S = 1$ (spin triplet). The pair state is ${}^3P_0$. The threshold behavior is $\rho \sim \beta^{2\cdot 1+1} = \beta^3 \sim \delta^{3/2}$.

Case 2 (pseudoscalar coupling). The pair must have $J^{PC} = 0^{-+}$. From $P = (-1)^{L+1} = -1$, we need L even. The minimum is $L = 0$. For $J = 0$ with $L = 0$: $S = 0$ (spin singlet). The pair state is ${}^1S_0$. The threshold behavior is $\rho \sim \beta^{2\cdot 0+1} = \beta \sim \delta^{1/2}$.

4.4 Corollary: range suppression

For scalar coupling to a fermion pair, the centrifugal barrier from $L = 1$ adds one full power of δ to the spectral function compared to S-wave. By the Laplace-transform argument (Section 5), this translates to one extra power of $1/r$ in the position-space potential tail:

Coupling	L	α	Tail
Scalar $\bar{\psi}\psi$	1	3/2	$e^{-2m_f r}/r^{7/2}$
Pseudoscalar $\bar{\psi}\gamma^5\psi$	0	1/2	$e^{-2m_f r}/r^{5/2}$
Scalar pair $\lvert\chi\rvert^2$	0	1/2	$e^{-2mr}/r^{5/2}$

The extra suppression for scalar coupling is a *direct consequence* of the intrinsic parity of the fermion–antifermion system.

4.5 Extension to vector and axial couplings

The same analysis extends to higher-spin couplings:

Coupling	J^{PC}	$L_{\rm min}$	State	Threshold
$\bar\psi\psi$ (scalar)	0^{++}	1	$^3P_0$	$\delta^{3/2}$
$\bar\psi\gamma^5\psi$ (pseudo)	0^{-+}	0	$^1S_0$	$\delta^{1/2}$
$\bar\psi\gamma^\mu\psi$ (vector)	1^{--}	0	$^3S_1$	$\delta^{1/2}$
$\bar\psi\gamma^\mu\gamma^5\psi$ (axial)	1^{++}	1	$^3P_1$	$\delta^{3/2}$

The pattern: couplings with **natural parity** ($P=(-1)^J$) force P-wave or higher; couplings with **unnatural parity** ($P=(-1)^{J+1}$) allow S-wave.

5 Position-Space Potential

[Long-distance tail] If the spectral function near threshold behaves as $\rho(\delta)\sim\delta^\alpha$, then the position-space potential at large r is

$$V(r)\sim-\frac{\mathrm{e}^{-2m_fr}}{r^{\alpha+2}}. \tag{11}$$

Near threshold, set $s=4m_f^2+\delta$ with $\sqrt{s}\approx 2m_f+\delta/(4m_f)$. Substituting into (2):

$$V(r)\sim-\frac{\mathrm{e}^{-2m_fr}}{4\pi r}\int_0^\infty\frac{\mathrm{d}\delta}{2\pi}\,\delta^\alpha\,\mathrm{e}^{-\delta r/(4m_f)}. \tag{12}$$

The Laplace transform gives (verified symbolically, Appendix A):

$$\int_0^\infty\delta^\alpha\,\mathrm{e}^{-\delta r/(4m_f)}\,\mathrm{d}\delta=\Gamma(\alpha{+}1)\left(\frac{4m_f}{r}\right)^{\alpha+1}. \tag{13}$$

Including the $1/(4\pi r)$ kernel: $V(r)\sim\mathrm{e}^{-2m_fr}/r^{\alpha+2}$.

5.1 Numerical verification

The position-space tails are verified by computing $V(r)$ from the spectral integral and fitting the power law of $|V|\cdot r\cdot\mathrm{e}^{2m_fr}$ vs. r:

Potential	Measured p	Theory (α+2)
Fermion, scalar coupling	3.79	$7/2=3.50$
Fermion, pseudoscalar	2.48	$5/2=2.50$
Scalar loop	2.56	$5/2=2.50$

The fermion scalar coupling gives a steeper tail than both the pseudoscalar coupling and the scalar loop, confirming the parity-forced barrier mechanism.

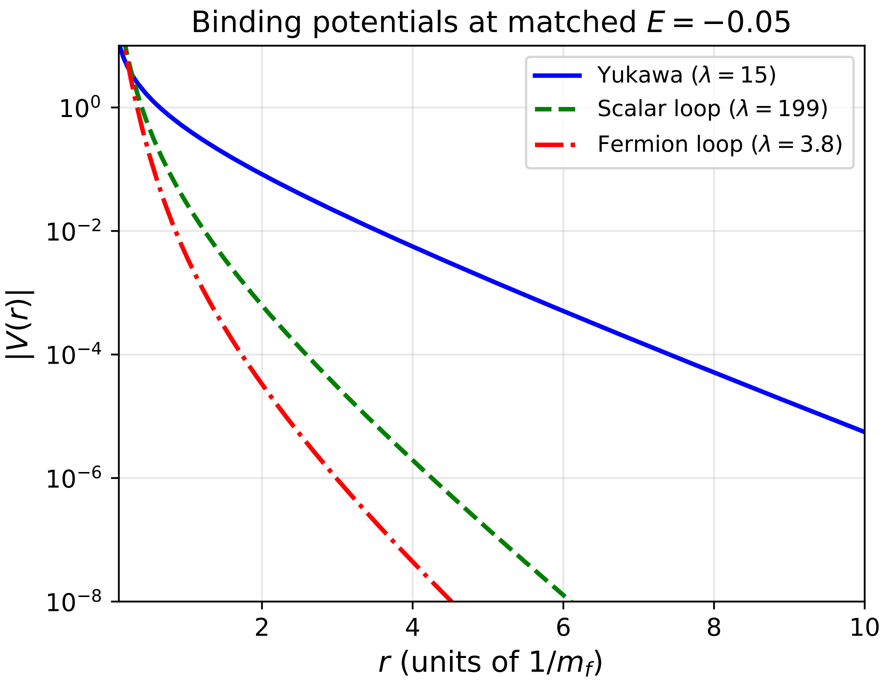

Figure 2: Binding potentials at matched binding energy $E = -0.05$. The coupling λ is tuned for each potential type to produce the same ground-state energy. The fermion-loop potential is more localized (shorter range, steeper falloff) despite requiring a smaller coupling λ.

6 Bound-State Properties

6.1 Variational method

To compare the size of composites bound by different potentials, we use the variational method with the hydrogen-like trial wave function

$$u(r) = r\,\mathrm{e}^{-\alpha r}, \tag{14}$$

where α is the variational parameter. This gives analytic results for the observables:

$$T = \frac{\alpha^2}{2M_{\text{red}}}, \tag{15}$$

$$\langle r^2 \rangle = \frac{3}{\alpha^2}, \tag{16}$$

$$F_1(q^2) = \frac{1}{(1 + q^2/(4\alpha^2))^2} \qquad \text{(dipole form factor).} \tag{17}$$

The potential expectation value $\langle V \rangle$ is computed numerically for each potential type. The total energy $E(\alpha) = T + \lambda\langle V \rangle$ is minimized over α, and the coupling strength λ is tuned to match a target binding energy.

6.2 Results at matched binding energy

The following table shows the variational results for three potential types at binding energy $E = -0.05$ (in natural units $m_f = 1$):

Potential	λ	α	R_{rms}	$\langle r^2 \rangle$	$q_{1\%}$
Yukawa (tree boson)	1.5×10^1	0.833	2.079	4.32	0.118
Scalar loop	2.0×10^2	3.690	0.469	0.220	0.524
Fermion loop (scalar cpg)	3.8×10^0	4.829	0.359	0.129	0.686

Here $R_{\text{rms}} = \sqrt{\langle r^2 \rangle}$ is in units of $1/m_f$, and $q_{1\%}$ is the momentum transfer at which $|F_1 - 1| = 1\%$.

Key ratios (fermion / Yukawa):

- R_{rms}: 0.17 $\Rightarrow$ fermion composite is **5.8× smaller**
- $\langle r^2 \rangle$: 0.030 $\Rightarrow$ **34× suppressed**
- $q_{1\%}$: 5.8 $\Rightarrow$ need **5.8× higher momentum transfer** to resolve structure

Parity barrier effect (fermion / scalar loop): $R_{\text{fer}}/R_{\text{scl}} = 0.76$, confirming an additional $\sim 30\%$ size reduction from the parity-forced centrifugal barrier.

6.3 Scaling with binding energy

The size ratios are relatively stable across binding energies:

E	$R_{\text{fer}}/R_{\text{Yuk}}$	$\langle r^2 \rangle$ ratio	$q_{1\%}$ ratio	$R_{\text{fer}}/R_{\text{scl}}$
−0.01	0.128	0.016	7.8	0.76
−0.05	0.173	0.030	5.8	0.76
−0.10	0.203	0.041	4.9	0.77
−0.50	0.305	0.093	3.3	0.82

The suppression is strongest at weak binding (large composites), where the long-distance tail dominates the wave function (Figure 4).

7 Physical Implications

7.1 Calibration to pion

To set the mass scale, we identify the Yukawa composite with the pion ($R_{\text{rms}} = r_\pi = 0.659$ fm). This gives an implied mediator mass

$$m_f = \frac{R_{\text{Yuk}} \cdot \hbar c}{r_\pi} = \frac{2.079 \times 197.3 \text{ MeV fm}}{0.659 \text{ fm}} \approx 623 \text{ MeV}. \tag{18}$$

The fermion composite then has

$$r_{\text{fer}} = R_{\text{fer}} \cdot \frac{\hbar c}{m_f} = 0.359 \times \frac{197.3}{623} \text{ fm} \approx 0.114 \text{ fm}. \tag{19}$$

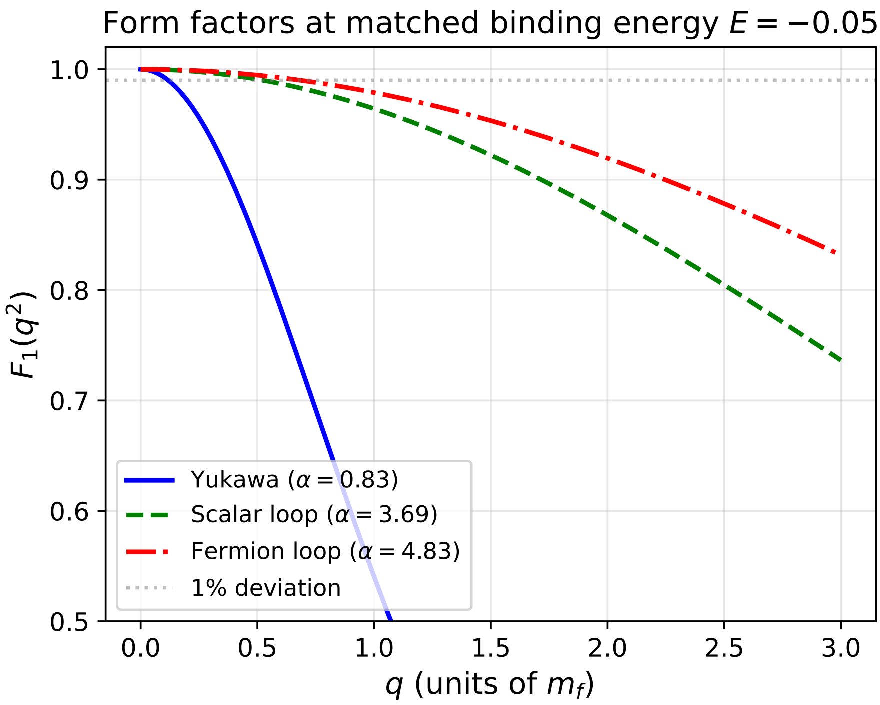

Figure 3: Form factors $F_1(q^2)$ at matched binding energy $E = -0.05$. The fermion-loop composite (red, dash-dot) stays close to the point-particle value $F_1 = 1$ over a much wider q range than the Yukawa composite (blue, solid).

7.2 Comparison to experimental limits

The experimental limit on muon compositeness from LEP contact-interaction analyses is $\Lambda > 8$ TeV, giving

$$r_\mu < \frac{\hbar c}{\Lambda} = \frac{197.3 \text{ MeV fm}}{8000 \text{ MeV}} \approx 0.025 \text{ fm}. \tag{20}$$

At the pion-calibrated scale ($m_f \approx 623$ MeV):

$$r_{\text{fer}} \approx 0.114 \text{ fm} \quad > \quad r_{\mu,\text{limit}} \approx 0.025 \text{ fm} \qquad \textbf{(detectable)}. \tag{21}$$

Thus, at QCD-scale mediator masses, even the fermionic composite would be visible. However, the composite size scales as $1/m_f$:

$$\langle r^2 \rangle (m_f) = \langle r^2 \rangle_{\text{ref}} \times \left(\frac{m_{f,\text{ref}}}{m_f} \right)^2. \tag{22}$$

7.3 Minimum mediator mass for undetectability

Setting $\langle r^2 \rangle (m_f) = \langle r^2 \rangle_{\text{limit}}$:

$$m_f^{\min} = m_{f,\text{ref}} \times \sqrt{\frac{\langle r^2 \rangle_{\text{ref}}}{\langle r^2 \rangle_{\text{limit}}}} = 623 \times \sqrt{\frac{0.0129}{6.08 \times 10^{-4}}} \approx 2900 \text{ MeV} \approx 2.9 \text{ GeV}. \tag{23}$$

For mediator masses above ~ 3 GeV, the fermion-exchange composite is below current experimental limits.

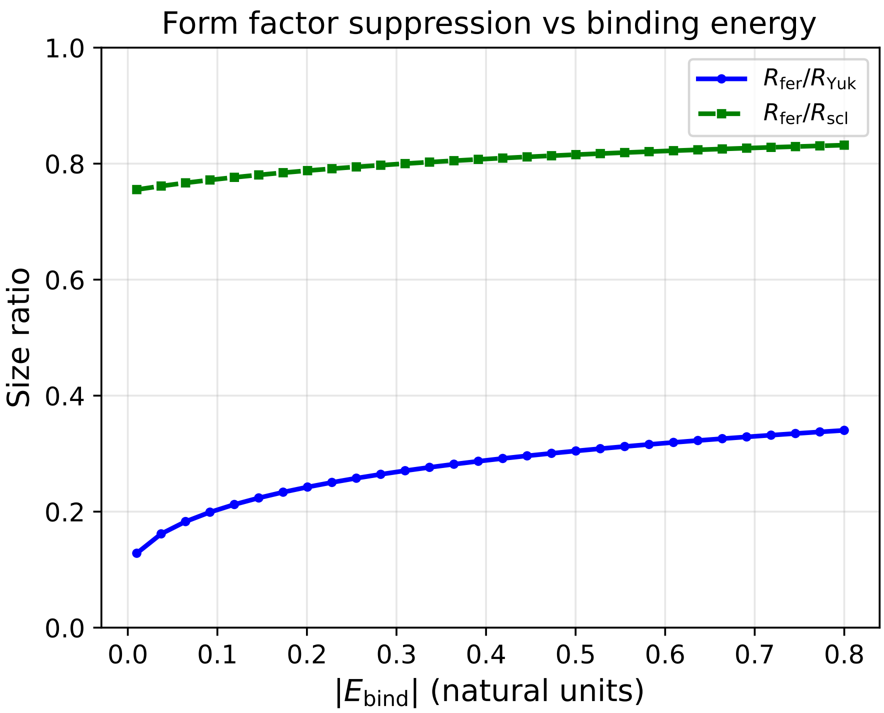

Figure 4: Size ratios vs. binding energy. The fermion-loop composite is always smaller than the Yukawa composite, with the suppression most pronounced at weak binding where the tail dominates.

7.4 At the electroweak scale

For a mediator at the electroweak scale ($m_f = 100$ GeV):

$$\langle r^2\rangle_{\mathrm{EW}} = 1.29 \times 10^{-2}\ \mathrm{fm}^2 \times \left(\frac{623}{10^5}\right)^2 \approx 5.0 \times 10^{-7}\ \mathrm{fm}^2, \tag{24}$$

which is $\sim 800\times$ below the experimental limit.

7.5 Form factor at experimental energies

The momentum transfer at which F_1 deviates from 1 by 1% is:

$$q_{1\%}^{\mathrm{Yuk}} = 0.118 \times 623\ \mathrm{MeV} \approx 74\ \mathrm{MeV}, \tag{25}$$

$$q_{1\%}^{\mathrm{fer}} = 0.686 \times 623\ \mathrm{MeV} \approx 427\ \mathrm{MeV}. \tag{26}$$

LEP operated at $q_{\max} \sim 100$ GeV, which is $234\times$ above the fermion composite's resolution scale at $m_f = 623$ MeV. At $m_f > 3$ GeV, the resolution scale exceeds LEP's reach.

8 Universality: Boson vs. Fermion Constituents

A natural question is whether the form factor suppression depends on the spin of the *constituents* (the particles being bound), or only on the spin of the *exchange* particle. We now show that the central potential—and hence the form factor at leading order—is universal: it depends only on the exchange mechanism.

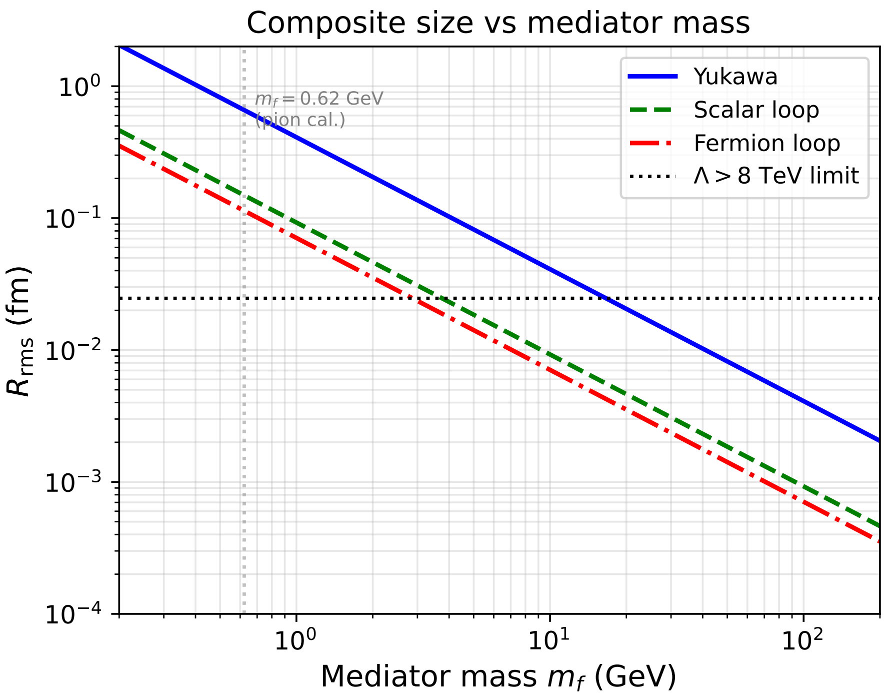

Figure 5: Composite charge radius vs. mediator mass. The horizontal line is the experimental muon compositeness limit ($\Lambda > 8$ TeV). At $m_f \gtrsim 3$ GeV, the fermion-loop composite drops below the limit.

8.1 Composite boson: two bosons + fermion exchange

This is the case analyzed in Sections 3–6. Two scalar sources ϕ_1, ϕ_2 interact via one-loop fermion pair exchange. The spectral function is $\rho_F(\delta) \propto \delta^{3/2}$, and the composite charge radius is $\sim 5.8\times$ smaller than Yukawa.

8.2 Composite fermion: two fermions + fermion exchange

Consider instead two fermionic constituents ψ_1, ψ_2 (like quarks) interacting via one-loop fermion exchange. In a SUSY context, this corresponds to quarks bound by gluino exchange (there is no direct quark–quark–gluino vertex in SUSY; the coupling goes through a squark, requiring at least one loop).

In the static limit, the external fermion propagators reduce to projectors onto the large components:

$$\bar{u}(p_1)\,\Gamma\,u(p_1) \to (2m_1)\,\delta_{s_1 s_1'} \times (\text{vertex factor}), \tag{27}$$

where Γ is the vertex structure. The spinor factors multiply the overall coupling but *do not modify the spectral function*, which is a property of the internal loop.

Therefore, the static central potential between fermionic sources has the **same spectral function** as between bosonic sources:

$$\rho^{(\text{fermion sources})}(s) = C_F \times \rho^{(\text{boson sources})}(s), \tag{28}$$

where C_F is a constant factor from the external spinor contractions. The threshold behavior, position-space tail, and form factor suppression ratio are all unchanged.

8.3 Spin-dependent corrections

For fermionic sources, the full (non-static) potential includes spin-dependent terms:

- **Spin-spin interaction**: $V_{SS}(r) \propto (\vec{\sigma}_1 \cdot \vec{\sigma}_2)\, f(r)$
- **Spin-orbit**: $V_{LS}(r) \propto (\vec{L} \cdot \vec{S})\, g(r)$
- **Tensor**: $V_T(r) \propto S_{12}\, h(r)$

These are suppressed by v^2/c^2 relative to the central potential in the non-relativistic limit. They split energy levels and affect the fine structure but do not qualitatively change the charge radius or form factor at the level of precision relevant here.

8.4 Summary of cases

Constituents	Exchange	Composite spin	R/R_{Yuk}
Boson + boson	Fermion pair (loop)	0	~ 0.17
Fermion + fermion	Fermion pair (loop)	0 or 1	~ 0.17
Fermion + boson	Fermion (tree?)	1/2	model-dependent
Boson + boson	Boson (tree)	0	1.00 (reference)
Fermion + fermion	Boson (tree)	0 or 1	~ 1.00

The form factor suppression is determined by the *exchange mechanism* (fermionic vs. bosonic), not by the constituent statistics. Any composite bound primarily by fermion-pair exchange will be ~ 5–$8\times$ smaller in R_{rms} (or ~ 30–$60\times$ smaller in $\langle r^2 \rangle$) than a bosonic-exchange composite of the same binding energy.

The one exception is the **fermion + boson** case with tree-level single-fermion exchange, which is possible when the vertex structure allows it. In this case, the dominant contribution is tree-level Yukawa (range $\sim 1/m_f$), and the composite is *not* unusually small.

9 Discussion

9.1 The action–angle perspective

The partial-wave theorem provides the rigorous content behind a qualitative "action–angle uncertainty" argument.

For bosonic exchange, the relevant uncertainty relation is $\Delta E \cdot \Delta t \gtrsim \hbar$ (or equivalently $\Delta p \cdot \Delta x \gtrsim \hbar$), where both E and t (or p and x) are unbounded. The only constraint on the range comes from the mediator mass: $R \sim 1/m$.

For fermionic exchange, the relevant conjugate pair involves the angular momentum (action) J and the angle φ: $\Delta J \cdot \Delta\varphi \gtrsim \hbar$. The angle is *compact* ($\varphi \in [0, 2\pi)$), so $\Delta\varphi$ is bounded. This means ΔJ cannot be made arbitrarily small: the fermion pair must carry at least the minimum orbital angular momentum allowed by parity.

The compactness of the angle variable is the root cause of the contact-like behavior: the conjugate momentum (action/angular momentum) is quantized and constrained, preventing the virtual fermion pair from spreading spatially.

9.2 Comparison of suppression mechanisms

Effect	Magnitude	Origin
Pair threshold	$2\times$ shorter range	Minimum mass $2m_f$
Parity barrier ($L = 1$)	$1.3\times$ smaller R	$P = (-1)^{L+1}$
Steeper tail ($r^{-7/2}$ vs r^{-1})	~ 3–$6\times$ smaller R	Spectral suppression
Total	**5.8× smaller R**	**(at matched binding energy)**

The dominant effect is the steeper position-space tail, followed by the range halving from the pair threshold. The parity barrier provides an additional $\sim 30\%$ suppression (comparing fermion scalar coupling to scalar loop, which share the same exponential range but differ by one power of $1/r$).

9.3 Model dependence

Our calculation uses a simple one-loop model with perturbative coupling. In a more realistic setting:

- **Non-perturbative effects**: Strong coupling could modify the spectral function away from threshold. However, the threshold behavior $\rho \sim \beta^{2L+1}$ is protected by kinematics (centrifugal barrier) and is non-perturbative.
- **Higher loops**: Multi-loop contributions have higher thresholds ($6m_f$, $8m_f$, ...) and are further suppressed.
- **Confinement**: If the fermions are confined (as in SUSY QCD with gluinos), the spectrum is discrete rather than continuous, but the lowest-lying exchange is still a fermion–antifermion composite (gluinoball), which is heavy and short-ranged.

10 Conclusion

We have shown that a composite particle bound by fermionic exchange is significantly more compact than one bound by bosonic exchange at the same mass scale and binding energy. The primary mechanism is the **parity-forced centrifugal barrier**: the intrinsic parity $(-1)^{L+1}$ of a fermion–antifermion pair forces P-wave at threshold for natural-parity couplings, adding a centrifugal barrier that suppresses the spectral function and steepens the position-space tail.

At matched binding energy, the fermion-exchange composite has:

- Charge radius $5.8\times$ smaller than Yukawa
- Mean-square radius $34\times$ suppressed
- Resolution scale $5.8\times$ higher in momentum transfer

For mediator masses above ~ 3 GeV, the composite is below current experimental limits on lepton compositeness ($\Lambda > 8$ TeV). At the electroweak scale ($m_f = 100$ GeV), the suppression is $\sim 800\times$ below the limit.

A muon-like particle can therefore be composite (as predicted by SUSY compositeness transfer from the pion) while appearing completely structureless in scattering, provided the mediating fermion is sufficiently heavy.

A Symbolic Verification

The following analytic results are verified symbolically using SymPy (script: `fermion/sympy_verify.py`):

1. **Scalar Feynman integral:** $\int_{x_-}^{x_+} [m^2 - x(1-x)s]\,\mathrm{d}x = -s\beta^3/6$. (Leading term $\propto \beta^3$.)
2. **Pseudoscalar Feynman integral:** $\int_{x_-}^{x_+} [m^2 + x(1-x)s]\,\mathrm{d}x = \beta(s + 8m^2)/6$. (Leading term $\propto \beta$.)
3. **Laplace transform:** $\int_0^\infty \delta^\alpha \mathrm{e}^{-b\delta}\,\mathrm{d}\delta = \Gamma(\alpha+1)/b^{\alpha+1}$.
4. **Threshold expansion:** $\beta(4m^2+\delta) = \sqrt{\delta}/(2m) - \delta^{3/2}/(16m^3) + \cdots$

5. **Dipole form factor:** $F_1(q) = [4\alpha^2/(4\alpha^2+q^2)]^2$ for trial $u = r\mathrm{e}^{-\alpha r}$.
6. **Charge radius:** $\langle r^2 \rangle = 3/\alpha^2$ (from both $-6\, F_1'(0)$ and direct integration).
7. **Yukawa expectation:** $\langle V_{\mathrm{Yuk}} \rangle = -\alpha^3/[\pi(2\alpha+\mu)^2]$.

B Numerical Scripts

All numerical results are reproduced by:

Script	Content
`fermion/fermionic_composite_form_factor_check.py`	Spectral exponents & tails
`fermion/is_it_a_point.py`	Variational bound states
`fermion/sympy_verify.py`	Symbolic verification

Requirements: Python 3.12, NumPy, SciPy, SymPy.

References

[1] R. L. Workman *et al.* (Particle Data Group), Prog. Theor. Exp. Phys. **2024**, 083C01 (2024).